Investigating the structural, mechanical and electronic stability of $Li_{7-x}La_3Zr_{2-x}Nb_xO_{12}$ garnet-type solid electrolyte

Khumbulani Tibane[1*], *Phuti* Ngoepe[1], *Raesibe* Ledwaba[1], and *Cliffton* Masedi[1]

[1]Materials Modelling Centre, University of Limpopo, Private Bag X1106, Sovenga 0727, South Africa

Abstract. The garnet-type oxide $Li_7La_3Zr_2O_{12}$ (LLZO) is considered a leading solid electrolyte for solid-state batteries due to its high lithium-ion conductivity and thermodynamic stability against lithium metal. However, at room temperature, LLZO forms a low-conductivity tetragonal phase. Supervalent doping has been demonstrated to induce lithium vacancies, thereby stabilizing the highly conductive cubic phase and enhancing structural stability. Despite extensive studies, the mechanistic understanding of supervalent substitution remains elusive. Therefore, in this study, density functional theory was employed to investigate the structural, mechanical, and electronic properties of pristine LLZO and niobium-doped $Li_{7-x}La_3Zr_{2-x}Nb_xO_{12}$ system with Nb concentration (x = 0.25). All systems were found to be thermodynamically and mechanically stable, satisfying Born stability criteria and exhibiting ductile behaviour. Phase transition was observed with Nb-doped content: a monoclinic phase at 12.5% ($Li_{6.75}La_3Zr_{1.75}Nb_{0.25}O_{12}$). Electronic structure analysis via density of states reveals that the doped system is an insulator, with a decreased band gap from 4.345 eV (pristine LLZO) to 3.734 eV upon doping. These findings substantiate the electronic stability and structural reconfigurability of Nb-doped LLZO systems.

1 Introduction

Energy storage technologies play a critical role in modern society, supporting a wide range of applications, including portable electronics, electric vehicles, and grid-scale energy storage systems. Various energy storage technologies differ in key parameters such as energy and power density, cycle life, efficiency, and economic feasibility. Among these, rechargeable battery systems have garnered significant attention due to their efficiency, scalability, and cost-effectiveness in energy storage applications [1, 2]. Solid-state lithium batteries have emerged as a promising advancement in battery technology, incorporating solid electrodes and a lithium-ion-conducting solid electrolyte. Unlike conventional lithium-ion batteries, which rely on flammable organic liquid electrolytes, solid-state lithium batteries mitigate the risk of thermal runaway and combustion by utilizing non-flammable solid-state electrolytes. This innovation enhances battery safety while simultaneously enabling higher

* Corresponding author: tibanekhumbulani01@gmail.com

energy densities and improved electrochemical stability. To achieve optimal performance, solid-state electrolytes must exhibit high lithium-ion conductivity, minimal electronic conductivity, and robust chemical stability in contact with electrode materials, ensuring long-term operational efficiency in rechargeable battery systems [3].

Among the diverse classes of solid-state electrolytes, including NASICON (Sodium Super Ionic Conductor) [4, 5], LISICON (Lithium Super Ionic Conductor) [6], perovskite [7], and garnet-type [8–10] materials, the garnet-structured lithium lanthanum zirconate ($Li_7La_3Zr_2O_{12}$, LLZO) has attracted considerable interest due to its superior ionic conductivity (~10^{-3} S cm^{-1} at room temperature) and wide electrochemical stability window (0–5 V vs. Li/Li^+) [3, 10]. These properties make LLZO a suitable candidate for next-generation solid-state lithium batteries, enabling compatibility with high-voltage cathodes and metallic lithium anodes. Additionally, LLZO exhibits excellent chemical and mechanical stability, further reinforcing its potential for application in advanced energy storage systems [11, 12]. Numerous elements have been investigated as dopants for the garnet-type LLZO solid electrolyte to enhance its structural and electrochemical properties. Substitution at the Li sites with elements such as Al, and Ga has been shown to influence the distribution and concentration of lithium ions within the crystal lattice, directly affecting ionic conductivity [13]. Similarly, partial substitution at the La and Zr sites with Sr, Ce, Mo, W, Ta, and Ti has demonstrated potential synergistic effects on lithium-ion mobility and structural stability [14, 15].

However, niobium (Nb) as a dopant at the Zr site remains underexplored, despite its significant potential. Nb is substantially less expensive than commonly used dopants like Ta or W, offering a cost-effective route for large-scale production of LLZO-based electrolytes. Moreover, Nb^{5+} may undergo partial reduction to lower oxidation states (Nb^{4+}, Nb^{3+}, Nb^{2+} and Nb^+) under certain electrochemical conditions, potentially enhancing the electronic conductivity of the electrolyte layer, which could be detrimental to solid electrolyte performance due to self-discharge during cycling [16]. Most studies have focused on enhancing the ionic conductivity of Nb-doped $Li_7La_3Zr_2O_{12}$ (LLZO) solid electrolytes. Among these, the composition with a Nb concentration of 12.5% (x = 0.25), corresponding to $Li_{6.75}La_3Zr_{1.75}Nb_{0.25}O_{12}$, has been identified as exhibiting the highest ionic conductivity (~8.0×10^{-4} S/cm at 25 °C) [17, 18]. This optimal doping level facilitates the stabilization of the cubic garnet structure and the creation of lithium vacancies, both of which are conducive to improved lithium-ion transport. Nevertheless, the structural stability of Nb-doped tetragonal LLZO under operating conditions remains insufficiently understood. Therefore, in this study, first-principles density functional theory (DFT) calculations are employed to investigate the structural, mechanical, and electronic properties of the pristine tetragonal LLZO and Nb-doped configuration. The goal is to elucidate the effects of Nb substitution at the Zr site on the structural stability and electronic characteristics of LLZO. This work contributes to the rational design of cost-effective garnet-type solid electrolytes suitable for all-solid-state lithium batteries.

2 Computational methodology

2.1 Crystal structure modelling of pristine LLZO

The atomic structure of pristine $Li_7La_3Zr_2O_{12}$ (LLZO) was modelled based on its experimentally determined crystallographic parameters. The tetragonal phase of LLZO crystallizes in the space group $I4_1/acd$ (No. 142), with a conventional unit cell containing 192 atoms. The atomic composition of the unit cell comprises 56 lithium (Li) atoms, 24 lanthanum (La) atoms, 16 zirconium (Zr) atoms, and 96 oxygen (O) atoms. In this unit cell

structure, lithium ions are distributed over distinct crystallographic sites: Li(1) occupies the tetrahedral 8a site, while Li(2) and Li(3) reside at distorted octahedral 16f and 32g sites, respectively. Lanthanum atoms, La(1) and La(2) are located at the 8b and 16e Wyckoff positions, while zirconium atoms occupy the 16c sites. Oxygen atoms are distributed among three crystallographically inequivalent sites: 32g, 32e, and 64h. A schematic representation of the LLZO crystal structure is presented in Figure 1, highlighting the arrangement and coordination of the constituent ions.

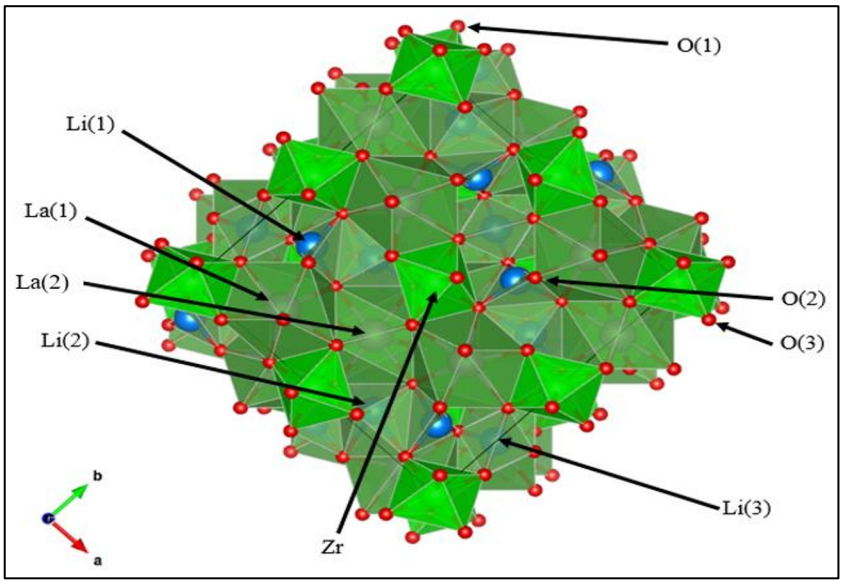

Fig. 1. Schematic crystal structure of tetragonal $Li_7La_3Zr_2O_{12}$. Tetrahedral Li(1) and distorted octahedral Li(2) and Li(3) sites are shown in the diagram.

2.2 DFT calculations with Vienna a*b initio* simulation package

The pristine LLZO and Nb-doped structures were modeled and evaluated using the density functional theory (DFT) calculations with the Vienna *ab initio* simulation package (VASP) code [19] to determine their structural, mechanical, and electronic stability. The simulations employed the projector-augmented wave (PAW) method [20] and the Perdew–Burke–Ernzerhof (PBE) [21] exchange-correlation functional within the generalized gradient approximation (GGA) to solve the Kohn–Sham equations, which describe the behaviour of electrons in a material. This approach ensures an accurate representation of the electronic structure and system properties. A plane-wave basis set with a cut-off energy of 500 eV was applied for both configurations. The Brillouin zone was sampled using the Monkhorst-Pack method with a 5x5x5 *k*-point mesh for the pristine and a 5x5x5 mesh for the Nb-doped structures. A force convergence threshold of 0.02 eV/Å was imposed to ensure precise geometry optimization. The mechanical and electronic property calculations were computed utilising the aforementioned plane-wave cut-off values and *k*-point mesh parameters.

2.3 Substitutional doping of niobium in LLZO

In this study, substitutional doping was employed to investigate the effects of niobium (Nb) incorporation into the LLZO ($Li_7La_3Zr_2O_{12}$) garnet-type structure. The Nb content was substituted at the Zr site to form $Li_{7-x}La_3Zr_{2-x}Nb_xO_{12}$, with doping concentrations of x = 0.25, 0.5, 0.75, and 1. This method is based on aliovalent substitution, where Nb^{5+} partially replaces Zr^{4+} within the crystal lattice. The substitution is expected to preserve the garnet structure while modifying the electronic environment and ionic conductivity of the LLZO. Charge compensation due to the aliovalent nature of Nb^{5+} substitution is achieved through the formation of Li vacancies as shown in Figure 2, which are known to facilitate Li^+ transport by enhancing the mobility of lithium ions within the lattice. This technique has been reported to contribute positively to the overall ionic conductivity of LLZO garnet-type solid electrolytes [22, 23].

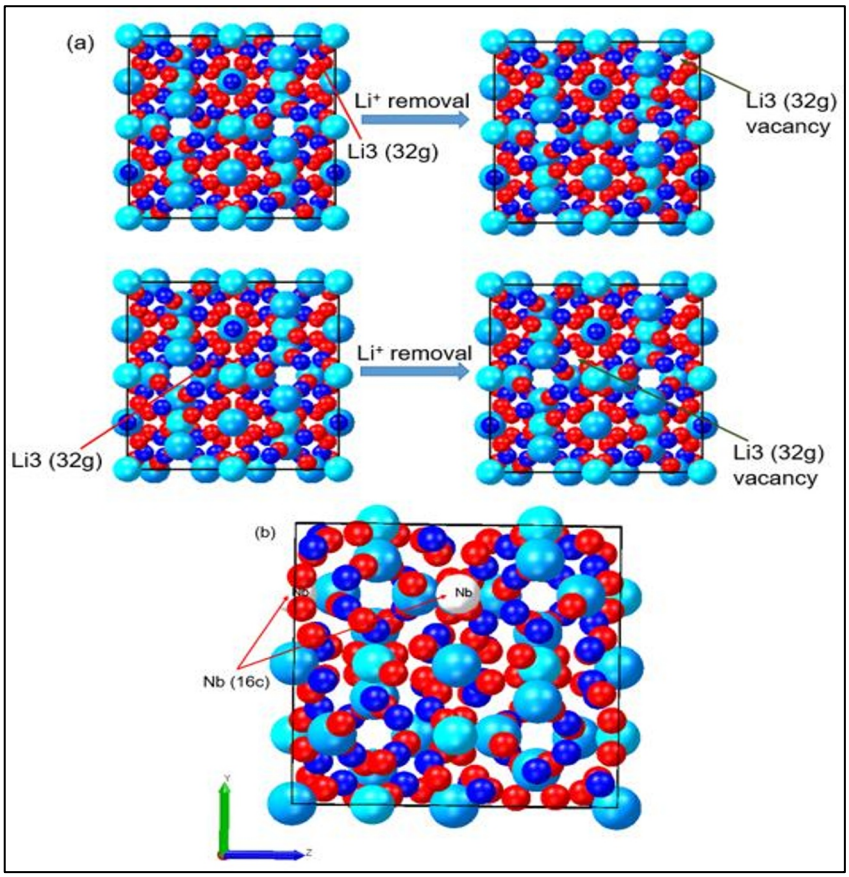

Fig. 2. Schematic representation of (a) lithium vacancy formation at the octahedral 32g site (Li3) crystallographic site and (b) niobium (Nb) substitution at the 16c site within the garnet lattice.

3 Results and discussion

3.1 Structural properties

The optimized lattice parameters for the tetragonal-phase $Li_7La_3Zr_2O_{12}$ (LLZO) structure are $a = b = 13.20$ Å and $c = 12.65$ Å. These values exhibit excellent agreement with experimental data ($a = b = 13.13$ Å and $c = 12.66$ Å)[19], corresponding to relative deviations of approximately 0.53% in the *a* and *b* directions and 0.08% along the *c* axis. Figure 3 illustrates the evolution of the lattice parameters (*a*, *b*, and *c*) as a function of Nb concentration in $Li_{7-x}La_3Zr_{2-x}Nb_xO_{12}$ (where x = 0.25) structure. As shown in Figure 3, the incorporation of Nb as a dopant in the pristine garnet structure induces a decrease in the lattice dimensions. Despite these structural modifications, the calculated heat of formation remains invariant at $\Delta H_f = -0.35$ eV/atom for Nb-doped composition, as indicated in Table 1. The consistent and negative formation energy indicates that pristine and doped structures are thermodynamically stable. This thermodynamic stability is crucial for maintaining structural integrity during repeated electrochemical cycling in battery applications. The similarity in ΔH_f between the pristine and Nb-doped LLZO further suggests that the substitution of Nb does not compromise the inherent stability of the host lattice.

Moreover, the doping process is inherently coupled with a structural transformation of the pristine LLZO, which alters its crystallographic framework. While the pristine crystallizes in the $I4_1/acd$ space group, Nb-substituted variant adopt lower-symmetry space group *P1*. The contraction of the lattice and reduction in symmetry due to Nb substitution are also influenced by the ionic radii of the substituent elements. Nb^{5+} (ionic radius ~0.64 Å in 6-fold coordination) is smaller than Zr^{4+} (~0.72 Å), which contributes to the observed lattice shrinkage upon doping. This size mismatch further drives local distortions and may alter the potential energy landscape for lithium diffusion. While the structural distortions could influence the percolation pathways for Li^+ ions, the maintained thermodynamic stability and reduced diffusion distances suggest that the Nb-doped structures remain promising for solid-state electrolyte applications.

Table 1. Lattice parameters (Å), heat of formation ΔHf (eV/atom) and volume (Å^3) of the pristine LLZO and the Nb-doped structures.

Composition	Lattice parameters (Å)	Heat of formation ΔH_f(eV/atom)	Volume (Å^3)	Space group
t-$Li_7La_3Zr_2O_{12}$ (Pristine)	a=13.20 c=12.65	-0.35	2203	$I4_1/acd$
Other [24]	a=13.12 c=12.66	-0.35	2203	$I4_1/acd$
Exp. [19]	a=13.13 c=12.66	-	2185	$I4_1/acd$
Nb-doped				
$Li_{6.75}La_3Zr_{1.75}Nb_{0.25}O_{12}$	a=13.10 b=12.79 c=13.13	-0.35	2200	P1

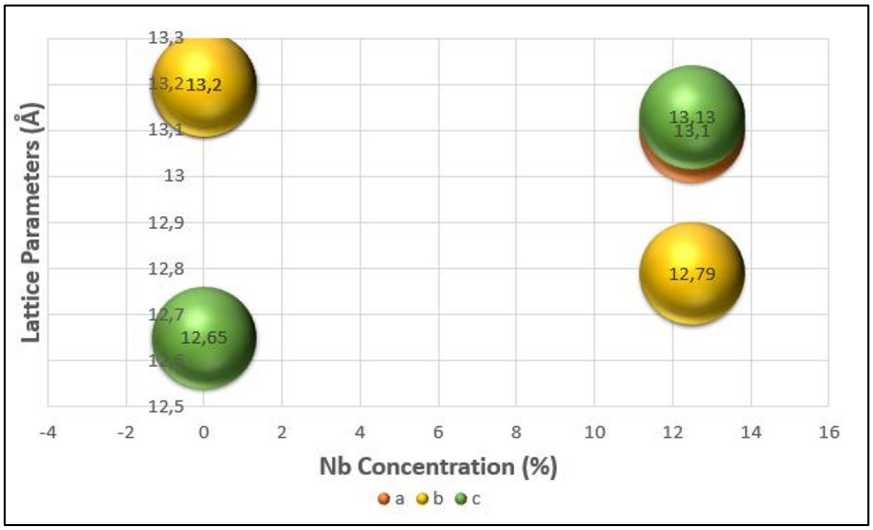

Fig. 3. Lattice parameters of the pristine LLZO and niobium-doped LLZO variant with 12.5% Nb content.

3.2 Mechanical properties

3.2.1 Elastic constants

Elastic constants, or elastic coefficients, are fundamental parameters for assessing the mechanical stability of crystalline materials. They quantify the stiffness of a material by describing its response to external stress and its ability to recover its original shape after deformation [25]. In the garnet-type $Li_7La_3Zr_2O_{12}$ (LLZO) solid electrolytes, these coefficients directly influence fracture resistance, dendrite suppression, and interfacial durability under the mechanical stresses encountered in all-solid-state batteries [26]. Accurate determination of elastic constants provides insight into the mechanical stability, influencing the performance and reliability of these materials in electrochemical devices. Table 2 presents the computed elastic constants for pristine tetragonal LLZO and Nb-doped structure, $Li_{7-x}La_3Zr_{2-x}Nb_xO_{12}$ (x = 0.25). At x = 0 ($Li_7La_3Zr_2O_{12}$), a tetragonal phase is observed, whereas at x = 0.25 ($Li_{6.75}La_3Zr_{1.75}Nb_{0.25}O_{12}$), a monoclinic phase is present. In crystalline materials, the number of independent elastic constants (C_{ij}) is determined by the symmetry of the system. A tetragonal crystal system exhibits six independent elastic constants: C_{11}, C_{12}, C_{13}, C_{33}, C_{44}, and C_{66}. While a monoclinic system, which possesses the lowest symmetry, requires thirteen independent elastic constants: C_{11}, C_{12}, C_{13}, C_{15}, C_{22}, C_{23}, C_{25}, C_{33}, C_{35}, C_{44}, C_{46}, C_{55}, and C_{66}.

The computed elastic constants for the pristine LLZO are in excellent agreement with prior literature reports [27], thereby validating the employed computational protocol. The composite shear constant C′ = (C11 – C12)/2 rises from 46.13 GPa to 47.11 GPa in the Nb-doped configuration, suggesting a net increase in structural rigidity with Nb doping. The positive C' values indicate the mechanical stability of all the systems, suggesting that they can withstand applied stresses without significant deformation or failure. Moreover, the pristine LLZO structure satisfy the mechanical stability criteria for a tetragonal crystal system, as defined by Equation 1. The Nb-doped composition $Li_{6.75}La_3Zr_{1.75}Nb_{0.25}O_{12}$ meet the mechanical stability criteria associated with a monoclinic system, as specified in Equation

3. The mechanical stability conditions for a tetragonal crystal system are defined as follows [28]:

$$C_{11} > |C_{12}|,$$

$$2C^2_{13} < C_{33}(C_{11} + C_{12}),$$

$$C_{44} > 0,\ 2C^2_{16} < C_{66}(C_{11} - C_{12}). \quad (1)$$

along with the positive definiteness of the elastic constants:

$$C_{11} > 0,\ C_{12} > 0,\ C_{13} > 0,\ C_{16} > 0,\ C_{33} > 0,\ C_{44} > 0 \text{ and } C_{66} > 0. \quad (2)$$

For a monoclinic system, the mechanical stability conditions are given by:

$$C_{44}C_{66} - C^2_{46} > 0,$$

$$C_{22} + C_{33} - C^2_{23} > 0,$$

$$C_{11} + C_{22} + C_{33} + 2(C_{12} + C_{13} + C_{23}) > 0,$$

$$C_{11} > 0,\ C_{22} > 0,\ C_{33} > 0,\ C_{44} > 0,\ C_{55} > 0,\ C_{66} > 0. \quad (3)$$

Table 2. Elastic constants of the pristine t-LLZO and the Nb-doped structures.

Elastic constants	t-$Li_7La_3Zr_2O_{12}$ (Pristine) (GPa)	Other [27] (GPa)	Nb-doped (GPa)
			P1
C_{11}	177.70	177.69	176.82
C_{12}	85.44	85.46	82.60
C_{13}	80.44	80.42	86.33
C_{15}	-	-	0.19
C_{22}	-	-	187.39
C_{23}	-	-	82.31
C_{25}	-	-	0.20
C_{33}	204.86	205.05	176.47
C_{35}	-	-	-0.54
C_{44}	76.51	76.51	74.54
C_{46}	-	-	0.20
C_{55}	-	-	68.69
C_{66}	71.27	71.27	77.32
C’	46.13	46.12	47.11

3.2.2 Elastic modulus

The mechanical behaviour of solid electrolytes under various stress conditions is critical for their performance and reliability in electrochemical systems, particularly in solid-state batteries. Solid electrolytes such as the garnet-type LLZO oxides are exposed to complex stress states during fabrication, assembly, and operation. These include volumetric compression induced by external stack pressure, shear stresses arising from interfacial mismatch with electrodes or dendrite propagation, and tensile/compressive stresses caused by volume changes during cycling. The elastic response of LLZO under such stress regimes

is essential for assessing its mechanical stability and fracture resistance. To characterize the elastic moduli of the pristine LLZO and niobium-doped structures, three fundamental mechanical moduli are evaluated: the bulk (B), shear (G), and Young's (E) moduli are critical parameters used to characterize the mechanical stability of materials under different stress conditions. These moduli reflect the response of the material to various types of deformation: bulk modulus measures resistance to uniform compression, shear modulus quantifies resistance to deformation under shear stress, and Young's modulus indicates the material's ability to withstand tensile or compressive forces.

The mechanical moduli for the pristine LLZO and Nb-doped structures are presented in Table 3. The bulk modulus (B), shear modulus (G), and Young's modulus (E) for pristine t-LLZO are computed as 113.99 GPa, 65.79 GPa, and 166.21 GPa, respectively, which exhibit good agreement with previous reports [27]. The Pugh's ratio [29] (B/G) of 1.78 and Poisson's ratio [30] (ν) of 0.26 indicate that pristine LLZO lies near the ductile–brittle transition limit: values above B/G>1.75 are indicative of ductile behaviour, whereas lower values suggest brittleness. For the Nb-doped system (*P1* composition), a slight increase in the bulk modulus to 115.89 GPa is observed, suggesting enhanced resistance to volume deformation upon substitution. However, the shear and Young's moduli decrease to 61.99 GPa and 157.82 GPa, respectively, indicating reduced resistance to shape deformation and overall stiffness. The increased B/G ratio (1.87) and Poisson's ratio (0.27) in the doped system suggest a transition towards more ductile behavior compared to pristine LLZO. This mechanical softening is likely attributable to local structural relaxations and lattice distortions introduced by Nb substitution at the Zr site, which can modulate interatomic bonding characteristics. Thus, Nb-doping in LLZO enhances ductility without substantially compromising compressive strength or structural stability, making it a promising strategy to improve the mechanical performance of pristine LLZO solid electrolytes.

Table 3. The bulk, shear, and Young's modulus, Pugh and Poisson's ratios of the pristine LLZO and the Nb-doped structures.

Moduli	Bulk (B)	Shear (G)	Young's (E)	Pugh ratio B/G	Poisson's ratio *v*
t-$Li_7La_3Zr_2O_{12}$ (Pristine)	113.99	65.79	166.21	1.78	0.26
Other [27]	112.23	64.84	163.51	1.73	0.26
Nb-doped					
P1	115.89	61.99	157.82	1.87	0.27

3.3 Electronic properties

3.3.1 Density of states

The density of states (DOS) is a fundamental tool in solid-state and condensed matter physics, providing critical insights into the electronic structure of materials and enabling the classification of their conductive behaviour as metallic, semiconducting, or insulating [31]. Analysis of the DOS provides critical insights into the distribution and occupancy of electronic states, thereby advancing the fundamental understanding of the electronic structure of the material. The DOS analysis of Nb-doped $Li_7La_3Zr_2O_{12}$ (Nb-LLZO) is crucial for elucidating the modifications in the electronic environment induced by niobium incorporation, the resulting influence on the band gap, and the subsequent impact on the material's performance as a solid-state electrolyte. Figure 4 presents the total DOS for the

pristine $Li_7La_3Zr_2O_{12}$ (LLZO) and the Nb-doped structures, with the atomic contributions clearly delineated. The analysis near the Fermi level reveals that pristine LLZO behaves as an insulator, exhibiting a direct band gap of 4.345 eV. This relatively wide band gap suggests that high-energy photons, corresponding to shorter wavelengths, are required to excite electrons from the valence band to the conduction band. Such electronic characteristics are particularly important for solid-state battery applications, where a wide band gap acts as an effective barrier to electronic leakage. By limiting unintended electron conduction, the LLZO structure enhances battery efficiency and stability, as electronic leakage often leads to self-discharge and degradation over time [10, 32].

The incorporation of niobium (Nb) as a dopant at the zirconium site in LLZO induces significant modifications to the electronic properties. The DOS profile for Nb-doped composition exhibit à direct band gap of 3.734 eV. The observed reduction in band gap for Nb-doped composition can be attributed to the synergistic effects of lithium vacancy formation and the substitution of Zr^{4+} by Nb^{5+}, both of which alter the local bonding environment and the distribution of electronic states near the Fermi level. Despite the reduction in band gap, the Nb-doped LLZO structure maintain insulating characteristics, as evidenced by the preservation of a finite band gap and the absence of electronic states at the Fermi level. This retention of insulating behaviour is critical, ensuring that the materials do not exhibit metallic conductivity, which would be detrimental to their function as solid-state electrolytes. The slight enhancement of electronic conductivity, without transition to metallicity, could facilitate improved interfacial charge transfer kinetics, potentially enhancing overall electrochemical performance without compromising the garnet-type LLZO's essential ionic transport properties. Moreover, A lower band gap implies that less energy is required for electron excitation, potentially improving interfacial charge transfer kinetics. Although high electronic conductivity is generally unfavorable for solid electrolyte applications, controlled doping strategies that modestly reduce the band gap without inducing metallic behaviour can optimize the delicate balance between ionic and electronic contributions.

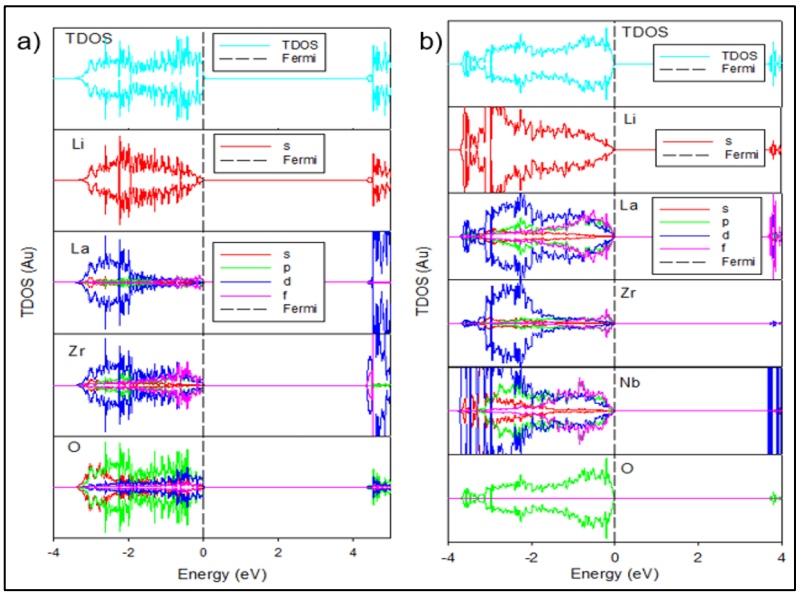

Fig. 4. The density of states of the (a) pristine tetragonal phase ($I4_1/acd$) $Li_7La_3Zr_2O_{12}$ (LLZO) and (b) monoclinic phase (*P1*) $Li_{6.75}La_3Zr_{1.75}Nb_{0.25}O_{12}$.

4 Conclusion

First-principles density functional theory (DFT) simulations utilising the PAW–PBE formalism in VASP were successfully employed to investigate the effects of supervalent Nb-doping ($Li_{7-x}La_3Zr_{2-x}Nb_xO_{12}$, x = 0.25) on the structural, mechanical, and electronic properties of the tetragonal $Li_7La_3Zr_2O_{12}$ garnet-type solid electrolyte. The pristine LLZO structure was determined to be thermodynamically stable, exhibiting good agreement with experimental data, with deviations of less than 1%. Substitutional doping of Nb^{5+} at Zr^{4+} sites introduced charge-compensating lithium vacancies, leading to contraction of the lattice parameters and reduction in crystal symmetry without compromising thermodynamic stability. Mechanical property analyses demonstrated that Nb doping generally enhanced the axial stiffness and composite shear resistance (C'), while slightly reducing shear moduli compared to the pristine phase. These changes contributed to improved structural rigidity, crucial for maintaining mechanical stability under the stresses encountered in solid-state battery applications. It is further observed that all compositions, tetragonal (x = 0 [pristine]) and monoclinic (x = 0.25), satisfy the mechanical stability criteria for their respective symmetries. Moreover, bulk, shear, and Young's moduli computations revealed that Nb incorporation preserved mechanical stability while imparting improved ductility, as evidenced by increases in Pugh's ratio (B/G > 1.75) and consistently high Poisson's ratio values. Thus, $Li_{6.75}La_3Zr_{1.75}Nb_{0.25}O_{12}$ (x = 0.25) reached the Pugh ratio value of 1.87, compared to 1.78 for the pristine structure. Electronically, Nb-doping reduces the direct band gap from 4.345 eV in pristine LLZO to 3.734 eV upon doping. However, the doped structure maintained its insulating nature, with no metallic states observed at the Fermi level. This preservation of insulating behaviour ensures that Nb doping does not adversely affect the electrolyte's electronic isolation, while a slightly reduced band gap may enhance interfacial charge transfer kinetics, potentially improving overall electrochemical performance. The reduction in band gap is advantageous for enhancing interfacial charge transfer and may improve the overall electrochemical performance in solid-state battery applications. This study demonstrates that Nb doping in LLZO effectively tunes the structural, mechanical, and electronic properties without compromising thermodynamic or mechanical stability. These findings highlight the potential of Nb-doped LLZO as a mechanically resilient, structurally stable, and electronically favorable solid electrolyte for next-generation all-solid-state lithium batteries.

The authors acknowledge the computational resources provided by the Materials Modelling Centre (MMC) at the University of Limpopo, as well as the Centre for High Performance Computing (CHPC) and the National Integrated Cyberinfrastructure System (NICIS) in Cape Town, South Africa.

The authors gratefully acknowledge financial support from the National Research Foundation (NRF) of South Africa under grant number PMDS230524109435, which provided essential resources enabling the successful completion of this study.

The datasets supporting the conclusions of this study can be obtained from the corresponding author upon reasonable request. The corresponding author will also provide additional supporting information, computational input files, and relevant experimental protocols upon justified inquiry, subject to availability and institutional data-sharing policies.

References

1. K.V. Kravchyk, D.T. Karabay, M.V. Kovalenko, On the feasibility of all-solid-state batteries with LLZO as a single electrolyte, Sci. Rep., **12**, 1177(1)-(10) (2022). https://doi.org/10.1038/s41598-022-05141-x

2. X.B. Cheng, R. Zhang, C.Z. Zhao, Q. Zhang, Toward Safe Lithium Metal Anode in Rechargeable Batteries: A Review, Chem. Rev., **117**, 10403-10473 (2017). https://doi.org/10.1021/acs.chemrev.7b00115
3. M. Kotobuki, H. Munakata, K. Kanamura, Y. Sato, T. Yoshida, Compatibility of Li 7 La3 Zr 2 O 12 Solid Electrolyte to All-Solid-State Battery Using Li Metal Anode, JES., **157**, A1076(1)-(4) (2010). https://doi.org/10.1149/1.3474232
4. Y. Zhu, X. He, Y. Mo, Origin of Outstanding Stability in the Lithium Solid Electrolyte Materials: Insights from Thermodynamic Analyses Based on First-Principles Calculations, ACS Appl. Mater. Interfaces., **7**, 23685-23693 (2015). https://doi.org/10.1021/acsami.5b07517
5. J.W. Fergus, Ion transport in sodium ion conducting solid electrolytes, Solid State Ion., **227**, 102-112 (2012). https://doi.org/10.1016/j.ssi.2012.09.019
6. T. Okumura, S. Taminato, Y. Miyazaki, M. Kitamura, T. Saito, T. Takeuchi, H. Kobayashi, LISICON-Based Amorphous Oxide for Bulk-Type All-Solid-State Lithium-Ion Battery, ACS Appl. Energy Mater., **3**, 3220-3229 (2020). https://dx.doi.org/10.1021/acsaem.9b01949?ref=pdf
7. S. Stramare, V. Thangadurai, W. Weppner, Lithium Lanthanum Titanates: A Review, Chem. Mater., **15**, 3974-3990 (2003). https://doi.org/10.1021/cm0300516
8. Y. Wang, A. Huq, W. Lai, Insight into lithium distribution in lithium-stuffed garnet oxides through neutron diffraction and atomistic simulation: Li7-xLa3Zr2-xTaxO12 (x = 0–2) series, Solid State Ion., **255**, 39-49 (2014). https://doi.org/10.1016/j.ssi.2013.11.017
9. V. Thangadurai, S. Narayanan, D. Pinzaru, Garnet-type solid-state fast Li ion conductors for Li batteries: critical review, Chem. Soc. Rev., **43**, 4714-4727 (2014). https://doi.org/10.1039/C4CS00020J
10. R. Murugan, V. Thangadurai, W. Weppner, Fast Lithium Ion Conduction in Garnet-Type Li7La3Zr2O12, Angew. Chem. Int. Ed., **46**, 7778-7781 (2007). https://doi.org/10.1002/anie.200701144
11. H. Duan, H. Zheng, Y. Zhou, B. Xu, H. Liu, Stability of garnet-type Li ion conductors: An overview, Solid State Ion., **318**, 45-53 (2018). https://doi.org/10.1016/j.ssi.2017.09.018
12. T. Yu, X. Yang, R. Yang, X. Bai, G. Xu, S. Zhao, Y. Duan, Y. Wu, J. Wang, Progress and perspectives on typical inorganic solid-state electrolytes, J. Alloys Compd., **885**, 161013(1)-(15) (2021). https://doi.org/10.1016/j.jallcom.2021.161013
13. D. Rettenwander, G. Redhammer, F. Preishuber-Pflügl, L. Cheng, L. Miara, R. Wagner, A. Welzl, F. Suard, M.M. Doeff, M. Wilkening, J. Fleig, Structural and electrochemical consequences of Al and Ga cosubstitution in Li7La3Zr2O12 solid electrolytes, Chem. Mat., **28**, 2384-2392 (2016). https://doi.org/10.1021/acs.chemmater.6b00579
14. S. Saran, Y.R. Eker, Synthesis, structural and conductive properties of Nd doped garnet-type Li7La3Zr2O12 Li-ion conductor, Curr. Appl. Phys.., **41**, 1-6 (2022). https://doi.org/10.1016/j.cap.2022.06.004
15. D.O. Shin, K. Oh, K.M. Kim, K.Y. Park, B. Lee, Y.G. Lee, K. Kang, Synergistic multi-doping effects on the Li7La3Zr2O12 solid electrolyte for fast lithium ion conduction, Sci. Rep., **5**, 1-9 (2015). https://doi.org/10.1038/srep18053
16. Y. Zhu, J.G. Connell, S. Tepavcevic, P. Zapol, R. Garcia-Mendez, N.J. Taylor, J. Sakamoto, B.J. Ingram, L.A. Curtiss, J.W. Freeland, D.D. Fong, Dopant-Dependent Stability of Garnet Solid Electrolyte Interfaces with Lithium Metal, Adv. Energy Mater., **9**, 1803440(1)-(11) (2019). https://doi.org/10.1002/aenm.201803440

17. E. Il'ina, Recent Strategies for Lithium-Ion Conductivity Improvement in Li7La3Zr2O12 Solid Electrolytes, Int. J. Mol. Sci.., **24**, 1-22 (2023). https://doi.org/10.3390/ijms241612905
18. N.H. Gaukås, T.O. Sunde, B. Arstad, A.H. Reksten, E. Stefan, A. Thøgersen, M.K. Pedersen, T. Norby, Y. Larring, Effects of Different Doping Strategies on Cubic Li7La3Zr2O12 Solid-State Li-Ion Battery Electrolytes, ACS Appl. Energy Mater.., **7**, 12141-12154 (2024). https://doi.org/10.1021/acsaem.4c02708
19. J. Awaka, N. Kijima, H. Hayakawa, J. Akimoto, Synthesis and structure analysis of tetragonal Li 7 La 3Zr 2O 12 with the garnet-related type structure, J. Solid State Chem., **182**, 2046-2052 (2009). https://doi.org/10.1016/j.jssc.2009.05.020
20. G. Kresse, J. Furthmüller, Efficient iterative schemes for ab initio total-energy calculations using a plane-wave basis set, Phys. Rev. B, **54**, 11169-11186 (1996). https://doi.org/10.1103/PhysRevB.54.11169
21. J.P. Perdew, K. Burke, M. Ernzerhof, Generalized Gradient Approximation Made Simple, Phys. Rev. Lett., **77**, 3865-3868 (1996). https://doi.org/10.1103/PhysRevLett.77.3865
22. P.E. Blöchl, O. Jepsen, O.K. Andersen, Improved tetrahedron method for Brillouin-zone integrations, Phys. Rev. B, **49**, 16223-16233 (1994). https://doi.org/10.1103/PhysRevB.49.16223
23. S. Yu, D.J. Siegel, Grain Boundary Contributions to Li-Ion Transport in the Solid Electrolyte Li 7La 3 Zr 2 O12 (LLZO), Chem. Mater.., **29**, 9639-9647 (2017). https://doi.org/10.1021/acs.chemmater.7b02805
24. S. Monismith, J. Qu, R. Dingreville, Grain-boundary fracture mechanisms in Li7La3Zr2O12 (LLZO) solid electrolytes: When phase transformation acts as a temperature-dependent toughening mechanism, J. Mech. Phys. Solids., **160**, 104791(1)-(15) (2022). https://doi.org/10.1016/j.jmps.2022.104791
25. J.F. Nye, (Oxford university press, 1985)
26. Y. Zhao, Y. Fu, B. Hu, C. Lü, Quaternized graphene oxide modified ionic cross-linked sulfonated polymer electrolyte composite proton exchange membranes with enhanced properties, Solid State Ion., **294**, 43-53 (2016). https://doi.org/10.1016/j.ssi.2016.07.002
27. R. Maphoto, M. Masedi, P. Ngoepe, R. Ledwaba, First-principles study on structural, mechanical and electronic properties of Li7La3Zr2O12 solid electrolyte, Suid-Afrikaanse Tydskrif vir Natuurwetenskap en Tegnologie, **40**, 12-15 (2021). https://hdl.handle.net/10520/ejc-aknat_v40_n1_a19
28. R. Mahlangu, M.J. Phasha, H.R. Chauke, P.E. Ngoepe, Structural, elastic and electronic properties of equiatomic PtTi as potential high-temperature shape memory alloy, Intermetallics., **33**, 27-32 (2013). http://dx.doi.org/10.1016/j.intermet.2012.09.021
29. S.F. Pugh, XCII. Relations between the elastic moduli and the plastic properties of polycrystalline pure metals, London Edinburgh Philos. Mag. & J. Sci., **45**, 823-843 (1954). https://doi.org/10.1080/14786440808520496
30. W.D. Callister Jr, D.G. Rethwisch, Wiley, (United State, 2020)
31. T. Phaahla, P. Ngoepe, H. Chauke, Exploring Synergistic Effect on the Stability of Ni-, Pd-, Ir-Doped TiN (N = 1–15) Nanoparticles, Alloy, **3**, 15-30 (2024). https://doi.org/10.3390/alloys3010002
32. V. Thangadurai, H. Kaack, W.J. Weppner, Novel Fast Lithium Ion Conduction in Garnet-Type Li 5La 3M 2O 12 (M = Nb, Ta), J. Am. Ceram. Soc.., **86**, 437-440 (2004). https://doi.org/10.1111/j.1151-2916.2003.tb03318.x